Effect of the mechanical properties on drilling resistance of Al$_2$O$_3$–TiO$_2$ coatings manufactured by atmospheric plasma spraying

C.C. Palacio [a,b,*], H. Ageorges [b], F. Vargas [c], A.F. Díaz [c]

[a] Universidad EAFIT, Applied Electromagnetism Research Group, Cra. 49 No. 7 sur 50, Medellin, Colombia
[b] University of Limoges, SPCTS, 123 Avenue Albert Thomas, 87060 Limoges, France
[c] University of Antioquia, GIPIMME, Street 67 No. 53, 108, Medellín, Colombia

ARTICLE INFO

ABSTRACT

Al$_2$O$_3$ with 13 and 45 wt.% TiO$_2$ microsized powders (6–22 and 13–41 μm for each chemical composition) were used as raw materials to coat AISI 1040 steel by atmospheric plasma spraying. The mechanical properties of the coatings were measured by micro-indentation tests, and drilling experiments were carried out using high speed steel (HSS) rotary drill bits of various diameters and varying the load on the drill bits. In order to reduce the effect of the wear on the bit, a new bit was used for each test. According to the results, the drilling test is proposed as a method of determining the mechanical properties of these coatings from the correlation found between coating hardness and drilling resistance.

© 2012 Elsevier B.V. All rights reserved.

1. Introduction

Drilling is a mechanical process widely used to perforate a material by cutting it by means of a rotary bit. The pierce resistance of a material is a function of its mechanical properties and as such can be used to measure its hardness. This process has been applied to metals successfully [1], but is not frequently used for ceramic coatings even if drilling tests have been carried out to characterize stone hardness versus depth and to evaluate stone treatments [2–4].

This cutting process involves the contact between the surface to be pierced and the drill bit so, therefore the drilling depth can be affected by the mechanical properties of the surface to be drilled, as well as the drilling parameters. This has motivated some researches that demonstrate that drilling resistance depends not only on the surface material hardness for ceramic materials such as stones [2–4], but also on the toughness, ductility and microstructure for surface treated steels [1].

Studies on alumina–titania coatings' drilling resistance [5] found that the phase and structure of the coating affected its mechanical properties. This was tested by comparing two different chemical composition of coatings (alumina with 13 wt.% and 45 wt.% of titania) formed using two different thermal spraying techniques (plasma and flame spraying).

The mechanical properties of materials deduced from instrumented drilling tests could be an attractive alternative to determine ceramic material hardness, toughness, and ductility. This would avoid the use of more time-consuming hardness tests, saving time and money when used in industry.

Building on previous research, the aim of this study is to evaluate the factors that affect the drilling resistance of alumina–titania coatings not considered before, such as the applied load during drilling test and the diameter of the drill bit and correlate these factors with the coating hardness by a mathematical model.

Currently, mechanical properties of ceramic coatings made by thermal spraying are measured using micro-indentation tests, also known as Vickers tests. In these tests, an indenter is pressed into the material, leaving an imprint. The length of the diagonals of the imprint on the material after indentation is measured, otherwise, the area of the indentation measured and related to a characteristic curve, which links the depth of the imprint and the load applied [6–13]. In the imprint produced by Vickers indentation, the elastic recuperation of the material may lead to overestimating the calculated hardness value. Accurate results from the Vickers test require knowledge of the elastic–plastic behavior of the material being tested then it is important to be able to identify the differences between elastic and plastic behavior [10], which in some cases is not reachable by direct observation and the results obtained keep as an approach. Researches on newer and simpler methods becomes interesting mainly if they are appropriate to obtain reproducible results useful to either quality control or compare mechanical resistances and stiffness of materials [6–8].

1.1. Experimental procedure

1.2. Experimental set up and spray parameters

The Atmospheric Plasma Spray (APS) coatings were manufactured using a Sultzer-Metco PTF4 torch, 7 mm anode-nozzle internal diameter, using a mixture of argon and hydrogen (45/15 L/min) as a plasma forming gas and a current intensity between 500 and 600 A. Powders were injected externally of the anode nozzle using an injector of 1.8 mm in internal diameter, positioned at 3 mm downstream of the

* Corresponding author. Tel.: +57 3104873704; fax: +57 42664284.
E-mail address: cpalac12@eafit.edu.co (C.C. Palacio).

torch nozzle-exit and at 8 mm from the torch axis. Particles were carried into the plasma jet by argon gas having a flow rate of 7 SLM and setting the powder flow rate in 30 g/min. The standoff distance was 100 mm. Prior to the injection of the powder, substrates were preheated to about 300 °C with the plasma jet.

1.3. Powders and coatings characterization

Size distribution of the particles used to form the coatings was determined by laser diffraction using a Malvern Master Sizer 2000.

The chemical composition of feedstock powders was determined using an ARL OPTIM'X™ spectrometer of Wavelength-Dispersive X-Ray Fluorescence (WD-XRF). Additionally, X Ray Diffraction (XRD) identified the phases present within both powders and coatings using SIEMENS D5000™ equipment. The percentages of crystalline phases were calculated by the Rietveld method using Maud software. The standard card numbers of Joint Committee on Powder Diffraction Standard (JCPDS) used to identify the phases present in feedstock materials and coatings were 01-0751864 for α-Al_2O_3, 00-029-0063 for γ-Al_2O_3, 01-070-1434 for Al_2TiO_5 and the Crystallography Open Database number — COD used to identify the $Al_6Ti_2O_{13}$ phase was 2014754.

The coatings' thicknesses and microstructures were evaluated on their cross sections using a JEOL JSM-6490LV and a PHILIPS XL30 Scanning Electron Microscopes (SEM). The cross sections were prepared by grinding using Buëhler APEX DGD Color grinds disk and then, polished with a cloth wetted in both 3 and 1 μm in diameter diamond paste, to obtain a smooth surface (Ra<0.1 μm). The defects in the structure of coatings were determined by image analysis, according to ASTM E1920-03 and E2109 standards [14,15], with a NIKON™ Optical Microscope. Images were processed with the Scion software.

The micro-hardness of coatings were calculated from twenty indentations carried out on the surface of each coating, using a Shimadzu Type M indenter, applying a load of 3.25 N during 15 s onto a Vickers indenter, according to ASTM C1327-99 Standard [9].

Drilling tests were conducted on the as sprayed surface of coating using a generic drill device retrofitted with a pneumatic automatic load system, a digital drill depth indicator, a jet of air to eject debris, a sample holder, and the HSS drill bits of varying diameters (6.35, 8.30 and 12.70 mm). It is presented in Fig. 1. The digital indicator allowed real time measurements of the drill and the pneumatic system controlled the load applied on the coated samples, which was kept fixed during each test on 390, 290 and 190 N of force. The diameter of the drill bits and the applied load were varied in order to produce different stress values on the coatings (each condition – diameter of the drill bit and applied load – was repeated three times) and then, these parameters
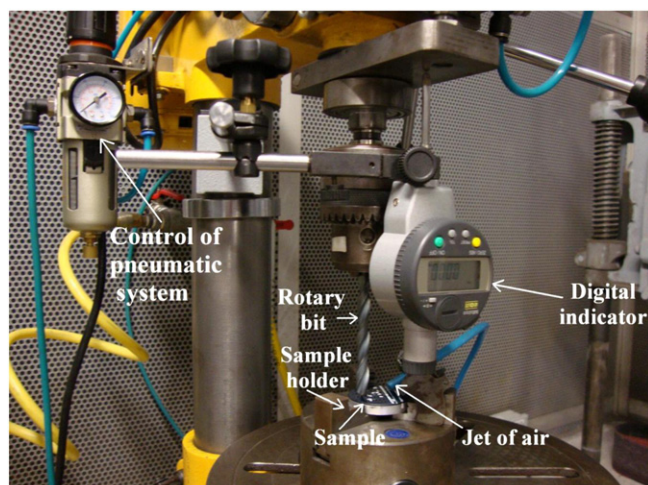
and the hardness of coatings were correlated to drill depth using Statistix [16] statistical software. In order to avoid the effect of wear on the drill bit, for each test a new bit was used. The rotational speed was set to 360 rpm, the pressure of the air jet to eject debris was 60 psi and the time for each test was fixed in 300 s.

1.4. Powders and substrates used

Four coatings using Atmospheric Plasma Spraying (APS) were fabricated from Saint Gobain SG-106™, SG-107™, SG-108™ and SG-109™ powders onto AISI 1040 steel substrates. Particles constituting the powders of alumina with 13 wt.% TiO_2, SG-106™ and SG-107™, had a size distribution between 13–41 and 6–22 μm respectively and the size distributions of the alumina powders with 45 wt.% TiO_2, SG-108™ and SG-109™, were 16–40 and 9–22 μm respectively (see Table 1). Particles of these powders had an irregular shape with fracture patterns in its surface indicating that they were produced by fusion and crushing.

The substrates were made of 6 mm thickness disk shaped AISI 1040 steel. Before spraying, they were grit-blasted with a corundum particle jet in order to achieve an average roughness Ra≈5 μm and then cleaned in a sonicated acetone bath to eliminate debris from the blast process.

1.5. Samples identification

To simplify the writing and the reading of the text, the coatings were codified as A and B according to their chemical composition, A being the AT-13 coatings fabricated from Al_2O_3–13 wt.% TiO_2 powders and B the AT-45 samples produced from Al_2O_3–45 wt.% TiO_2 powders. Additionally, numbers 1 and 2 are assigned according to the distribution sizes of the particles used as raw material, 1 being for coatings fabricated from coarser particles and 2 for coatings obtained from finer particles, this naming convention is illustrated in Table 1.

2. Results and discussion

2.1. Microstructures and thicknesses of the coatings

The structure of coatings presented in Fig. 2 is constituted by the classical characteristics of micrometer coatings as lamellas and non-connected defects as pores (globular and irregulars), cracks and partially melted particles. It was observed that the porosity content is higher in A coatings ($10.6\% \pm 1.4$ and $5.2 \pm 0.3\%$ for A1 and A2, respectively) fabricated from Al_2O_3–13 wt.% TiO_2 powders than in the B ones ($3.5 \pm 0.3\%$ and $3 \pm 0.6\%$ for B1 and B2, respectively) made of Al_2O_3–45 wt.% TiO_2 powders. The highest porosity content in A coatings is due to Al_2O_3–13 wt.% TiO_2 powders have higher melt point than Al_2O_3–45 wt.% TiO_2 powders used to produce B coatings. This reduces the fluidity of the sprayed particles for A coatings making difficult the splats formation and its homogeneous piling up. The presence of cracks is more evident in the coatings fabricated from coarser particles (A1 and B1) than those made of finer particles (A2 and B2) owing to a higher stress level produced by coarser particles.

Fig. 1. Device used to carry out the drilling tests.

Table 1
Chemical composition and distribution size of Al_2O_3/TiO_2 particles used.

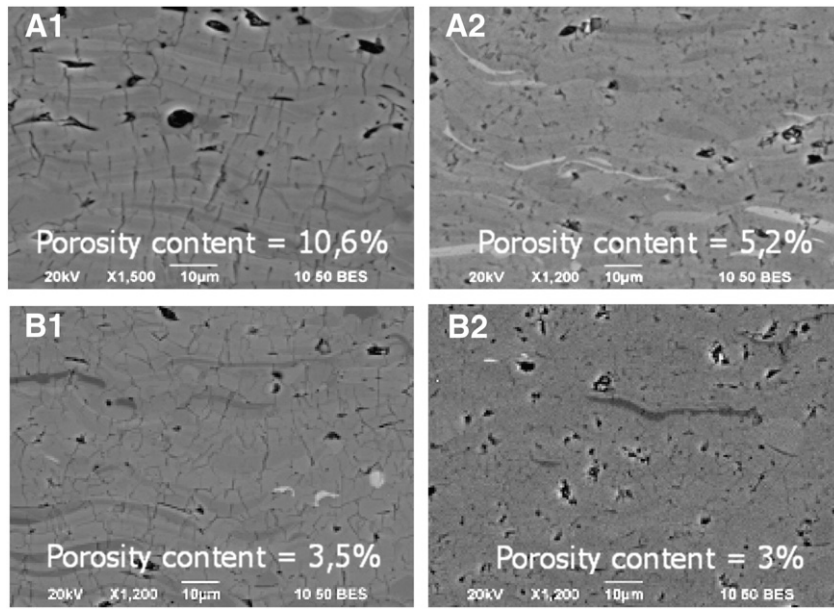| Raw material	Powder code	Chemical composition [wt.%]			Particles size distribution [μm]	
		Al_2O_3	TiO_2	Others	d_{10}	d_{90}
SG-106™	A1	83.9 ± 0.2	15.3 ± 0.2	0.8	13.0	41.2
SG-107™	A2	84.7 ± 0.2	14.3 ± 0.2	1.0	6.3	22.1
SG-108™	B1	50.3 ± 0.2	47.7 ± 0.2	2.0	15.9	39.8
SG-109™	B2	55.2 ± 0.2	43.1 ± 0.2	1.7	8.8	22.3

Fig. 2. Microstructures observed in coatings corresponding as follows: A1 to AT-13 coatings and 15–45 μm particles size of powders, A2 to AT-13 coatings and 5–30 μm particles size of powders, B1 to AT-45 coatings and 15–45 μm particles size of powders, B2 to AT-45 coatings and 5–30 μm particles size of powders.

Thicknesses of coatings were 1026 ± 11 μm onto A1, 1012 ± 31 μm onto A2, 904 ± 24 μm onto B1 and 875 ± 16 μm onto B2.

2.2. Phase analysis of the coatings

The phases in the coatings are presented in Table 2. Samples A1 and A2 are mainly constituted of both alpha alumina (α-Al_2O_3) and gamma alumina (γ-Al_2O_3) while in B1 and B2 coatings, tialite (Al_2TiO_5) and aluminum titanate ($Al_6Ti_2O_{13}$) are the present phases, which have lower hardness and mechanical resistance than alpha and gamma alumina [11–13]. These results are in accordance with the literature indicated that α-Al_2O_3 and γ-Al_2O_3 are the main phases present in hypoeutectic materials based on the Al_2O_3–TiO_2 system having a low TiO_2 content, while Al_2TiO_5 and $Al_6Ti_2O_{13}$ are the phases present in materials in eutectic or near to eutectic composition of the Al_2O_3–TiO_2 system [17–20].

2.3. Microhardness and drilling resistance of the coatings

The results obtained in the micro-indentation tests of the coatings are presented in Table 3. They show that the hardness of A1 and A2 samples, made from Al_2O_3–13 wt.% TiO_2 are higher than those of B1 and B2 coatings produced from Al_2O_3–45 wt.% TiO_2, which can be attributed to the high hardness of α-Al_2O_3 and γ-Al_2O_3 phases in A1 and A2 coatings. In spite of the fact that the hardness of α-Al_2O_3 is higher than the hardness of γ-Al_2O_3 [5], A2 coating exhibits higher hardness than A1 which has higher amount of α-Al_2O_3. This can be due to the influence of the porosity content higher in A1 than in A2 as Fig. 2 illustrates. The reduced

difference in the porosity contents of B1 and B2 coatings makes their hardness equals despite of the high difference in their phase's amount.

Drill test results were obtained by averaging the drill depth of various drill diameters and loads as Fig. 3 shows. The results indicate that samples A (AT-13 coatings) show lower drill depths than B coatings (AT-45 coatings) due to the presence of α-Al_2O_3 and γ-Al_2O_3 phases in A which have higher mechanical resistance than Al_2TiO_5 and $Al_6Ti_2O_{13}$ present in B [11–13]. The deviations of drilling resistances of A1 and A2 coatings are 14% minimum and 15% maximum for the bit effect and 6% minimum and 15% maximum for the load applied effect, while for B1 and B2 coatings are 5% minimum and 11% maximum for the bit effect and 11% minimum and 23% maximum for the load applied effect, like Fig. 3 illustrates. For high loads (>290 N) the drill depth is almost constant, which can be attributed to elastic deformation in the contact surface between the coating and the drill bit tip, reducing the effect of the drill bit on the coating. On the other hand, the higher the drill bit diameter, the lower the drill depth, because the stress applied is lower on the contact area.

The higher hardness in AT-13 coatings increases the wear in the drill bits used to perforate them, reducing the effectiveness of these tools on the coatings despite the appearance of the bit used to perforate the AT-45 coating which seems like larger due to the higher contact area produced on this material thanks to its lower hardness. Fig. 4 presents the representative drilling trace as well as the wear in the drill bits tip for each kind of coating tested, applying 390 N as load on a drill bit of 12.54 mm in diameter. The rotational indentation under high localized stress applied by HSS drill bits generates plastic deformation and detachment of particles from the coatings whereas layers of debris from the HSS drill bits were observed on the surface of imprints, mainly in those produced in AT-13 coatings.

Table 2
Phases content of the Al_2O_3–13 wt.% TiO_2 and Al_2O_3–45 wt.% TiO_2 APS coatings.

Sample code	Phase analysis	
	Phases	Weight %
A1	γ-Al_2O_3	92.8 ± 6.2
	α-Al_2O_3	7.2 ± 0.6
A2	γ-Al_2O_3	99.1 ± 0.9
	α-Al_2O_3	0.9 ± 0.3
B1	Al_2TiO_5	28.9 ± 2.7
	$Al_6Ti_2O_{13}$	71.1 ± 3.6
B2	Al_2TiO_5	55.2 ± 6.6
	$Al_6Ti_2O_{13}$	44.8 ± 2.2

Table 3
Vickers hardness of the Al_2O_3–13 wt.% TiO_2 and Al_2O_3–45 wt.% TiO_2 coatings.

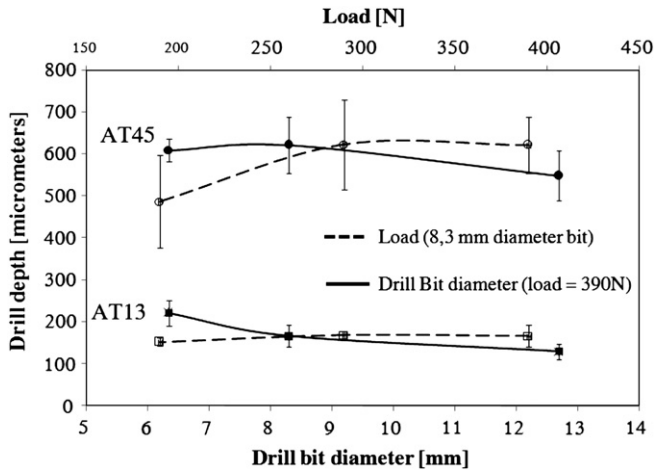| Sample code	$HV_{3.25\ N}$ [GPa]
A1	11.2 ± 1.2
A2	12.0 ± 1.2
B1	8.9 ± 0.9
B2	8.9 ± 0.6

Fig. 3. Effect of the load and diameter of the drill bit on drill depth in the Al_2O_3–13 wt.% TiO_2 and Al_2O_3–45 wt.% TiO_2 coatings.

The maximal drill depths observed in AT-45 coatings correspond to 71% of their thicknesses while in AT-13 coatings are 22%. This behavior of the coating approaches to bulk material and permits to neglect the substrate influence on drilling resistance.

The stochastic model presented in (Eq. (1)) was determined using the analytical software named Statistix. This software allows obtaining relationships between different experimental parameters that act as dependent and independent variables and afterwards makes possible a fit evaluation among the experimental data and the estimated model [16]. The following model was defined from results of micro-indentation and drilling tests and it describes the relationship between the hardness of coating, the load applied on the drill bit and its diameter, with the drill depth reached:

$$D_D = \frac{-0.5\ L^2 + 329\ L - 11,160}{0.00123\ HV^{4.8} \times \varphi_b^{0.2}} \qquad (1)$$

where

D_D	is the drill depth [μm]
L	is the load applied to the drill bit [N]
HV	is the hardness Vickers [GPa]
φ_b	is the drill bit diameter [mm]

The quality of the proposed model was evaluated by applying the fit's tests to both global model and specific variables in the equation by using different five statistic tests. These were carried out and gathered as follows: i) global model evaluation was conducted by the time series analysis and normal probability of the residuals calculated by (Eq. 1) and those obtained experimentally; ii) specific variable evaluations were conducted by determination of the residuals for each individual parameter (residuals of load, hardness and drill bit diameter). In all the cases an acceptable statistical fit condition was reached.

3. Conclusions

- Coatings of Al_2O_3–13 wt.% TiO_2 and Al_2O_3–45 wt.% TiO_2 were fabricated by atmospheric plasma spraying from powders of two different particle size distributions for each chemical composition. The hardness and drilling resistance were measured on the surface of coatings and results obtained allowed to correlate coating properties with drill test parameters.
- Drill depth increases while bit diameter decreases and applied load increases. This is due to the increase in stress caused by applying more force per unit area.
- Samples that have higher hardness value (Al_2O_3–13 wt.% TiO_2 coatings) exhibit higher drilling resistance (lower drill depth) due to the presence of hard phases as α alumina and γ alumina, which produces a high wear in the drill bit tip, thus reducing its effectiveness during the drilling test.
- The mechanical behavior of coatings during drilling resistance measures can be considered close to bulk materials due to the thicknesses of coatings were enough to avoid the substrate influence.
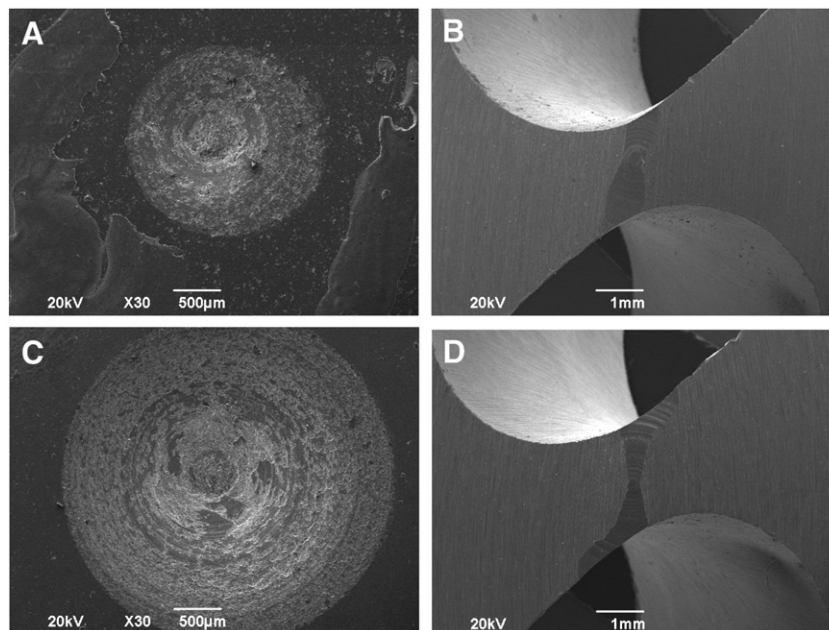

Fig. 4. Drill withdrawal produced on the surface of coatings and wear on the drill bit tip. (a) Track produced on AT-13 coatings, (b) wear observed in the tip of the drill bit used to perforate AT-13 coatings, (c) track produced on AT-45 coatings, (d) wear observed in the tip of the drill bit used to perforate AT-45 coatings.

References

[1] G. Mauvoisin, O. Bartier, R. El Abdi, A. Nayeb, Int. J. Mach. Tool Manuf. 43 (2003) 825.
[2] M. Pamplona, M. Kocher, R. Snethlage, L.A. Barros, in: 18_665_676_Pamplona.fm Seite 665 Dienstag, Z. dt. Ges. Geowiss, 158/3, 2007, p. 665.
[3] J. Delgado Rodrigues, D. Costa, Int. J. Restor. 10–3 (2004) 1.
[4] J. Delgado Rodrigues, A. Ferreira Pinto, D. Rodrigues da Costa, J. Cult. Herit. 3 (2002) 117.
[5] F. Vargas, Élaboration de couches céramiques épaisses à structures micrométriques et nanométriques par projection thermiques pour des applications tribologiques. Ph.D. thesis (2010), [in French], University of Limoges (France), 2010, 151–15.
[6] I.J. McColm, in: Ceramic Hardness, Plenum Press, New York and London, 1990, p. 46.
[7] W.C. Oliver, G.M. Pharr, Mater. Res. 7 (1992) 1564.
[8] J.M. Meza, C. Chaves, J.M. Vélez, Revista Dyna 73–149 (2006) 81.
[9] ASTM C1327, Standard Test Method for Vickers Indentation Hardness of Advanced Ceramics. ASTM, 1999.
[10] D. Chicot, I. Hage, P. Démarécaux, J. Lesage, Surf. Coat. Technol. 81 (1996) 269.
[11] F. Vargas, H. Ageorges, P. Fournier, P. Fauchais, M.E. López, Surf. Coat. Technol. 205–4 (2010) 1132.
[12] R. Yilmaz, A.O. Kurt, A. Demir, Z. Tatli, J. Eur. Ceram. Soc. 27 (2007) 1319.
[13] K.A. Habib, J.J. Saura, C. Ferrer, M.S. Damra, E. Giménez, L. Cabedo, Surf. Coat. Technol. 201 (2006) 1436.
[14] ASTM E1920-03, Guide for metallographic preparation of thermal sprayed coatings.
[15] ASTM E2109, Standard test methods for determining area percentage porosity in thermal sprayed coatings.
[16] Statistix, Analytical Software. Creation date: 2008. (last access date: February 6th/2012; http://www.statistix.com/features.html).
[17] J. Ilavski, C.C. Berndt, H. Herman, P. Chraska, J. Dubsky, J. Therm. Spray Technol. 6 (1997) 439.
[18] R. Venkataraman, B. Ravikumar, R. Krishnamurthy, D.K. Das, Surf. Coat. Technol. 201 (2006) 3087.
[19] M.H. Berger, A. Sayir, J. Eur. Ceram. Soc. 28 (2008) 2411.
[20] S. Hoffmann, S.T. Norberg, M. Yoshimura, J. Solid State Chem. 178 (2005) 2897.